

Retrofit for Blast-Resistant RC Slabs with Composite Materials

by B. Lu, P. Silva, A. Nanni, and J. Baird

Synopsis: This research program was initiated to examine the feasibility of assessing the blast-resistant capacity of reinforced concrete (RC) slabs using the displacement based design (DBD) method. In order to achieve this objective, five RC slabs were tested under real blast loads in the out-of-plane direction. One of the slabs was used as the control unit to establish a baseline for comparison in terms of performance for the other four slabs, which were strengthened with fiber reinforced polymer (FRP) and steel fiber reinforced polymer (SRP). The explosive charge weight and stand-off distance required to impose a given damage level were predicted by the DBD method. Test results showed that the blast loads were effectively estimated and the damage levels observed from the field tests correlated well with the predicted levels. In addition, test results corroborated that the blast-resistant capacity of RC slabs can be effectively increased by strengthening using FRP composites. The main conclusion that can be drawn from these tests using improvised explosive devices (IDE) is that RC slabs retrofitted on both sides have a higher blast resistance capacity than those slabs retrofitted only on one side. This paper discusses these experimental results along with the analysis steps used to predict the blast charge and standoff distance to impose a given damage level.

Keywords: blast-resistant; displacement-based method; ductility; fiber reinforced polymers; steel-reinforced polymers

1346 Lu et al.

Binggeng Lu is a graduate student at the Center for Infrastructure Engineering Studies (CIES) at the University of Missouri–Rolla (UMR). His research interests include the performance and evaluation of structures subjected to seismic and blast loads.

Pedro Franco Silva is an assistant professor of Civil Engineering in CIES at UMR. He received his PhD from the University of California-San Diego, Calif. His research interests include earthquake engineering and the seismic performance evaluation of bridge structures.

Antonio Nanni, FACI, is the V&M Jones Professor of Civil Engineering and Director of CIES at UMR. He is chair and member of ACI437, Strength Evaluation of Existing Concrete Structures; 440, Fiber Reinforced Polymer; Reinforcement; 544, Fiber Reinforced Concrete; 549, and Joint ACI-ASCE-TMS Committee. His research interests include performance of concrete-based structures.

Jason Baird, is a research assistant professor in the Department of Mining Engineering at UMR and the president of Loki, Inc. His research interests include blast optimization and design of blast-resistant structures.

INTRODUCTION

Recent events have drawn considerable attention to the vulnerability and sustainability of structural members subjected to improvised explosive devices (IED). Since protection is never an absolute concept and there is a level of high costs associated with a given damage level of protection, proper assessment tools must be employed to determine within a reasonable degree of accuracy the level of vulnerability of existing and new structures. Furthermore, in blast design, one must also determine an acceptable level of damage that a structure can tolerate. Explosive effects can impact a level of damage that can range from minor damage to completely structural failure and considerable loss of life (FEMA, 2003). This research program has shown promising results in using the DBD method to predict blast loads in terms of standoff distance and charge weight.

In this program, the performance of concrete slabs strengthened with carbon fiber reinforced polymers (CFRP) and a new class of composites composed of knitted high strength steel cords designated as steel reinforced polymers (SRP) (Wobbe et al., 2004) were investigated under real blast loads. Different retrofit schemes consisting of these CFRP and SRP strengthening schemes applied on one side and both sides of the tested slabs were investigated and results are discussed in this paper. In total five slabs with different strengthening schemes and materials were tested under real blast loads.

EXPERIMENTAL PROGRAM

Test Specimens

As shown in Figure 1, a series of square RC slabs with nominal dimensions of 1200 x 1200 x 90mm were chosen for the experimental and analytical investigation. Different materials and upgrade schemes were investigated against out-of-plane blast loads. Five RC slabs were built and strengthened with different schemes and different materials such as CFRP or SRP. With the exception of the control slab (1), two slabs (2A and 2B) were strengthened with CFRP laminates, and the other two (3A and 3B), were strengthened with SRP laminates. The strengthening schemes are also shown in Figure 1 and Table 1. Slabs 2A and 3A were strengthened on the bottom side only, whereas, slabs 2B and 3B were strengthened on both sides to evaluate the influence of negative moments developed under the dynamic response or negative overpressure.

The experimental specimens were tested at the experimental mine at the University of Missouri-Rolla. As shown in Figure 2a, it can be seen that the distance from the test specimen to the mine walls and ceiling are far enough apart that open air design methods are applicable within a reasonable degree of accuracy. As shown in Figure 2b, the test specimens were simply supported on steel box beams. The charge was suspended above the test specimens to the specific standoff distance by a wire, which was also used as the circuit to detonate the charge. Each charge was composed of desensitized RDX high explosive.

Material Properties and Moment-Curvature Relationships

The material properties are as follows. All the five specimens were poured with 28MPa concrete and reinforced with steel bars with a 0.18% reinforcement ratio in each direction. The steel grade was 410MPa with an elastic modulus of 200GPa. The CFRP and SRP laminates demonstrated an elastic behavior up to their ultimate tensile strengths, which were 3794MPa and 3199MPa, and the elastic moduli were 228GPa and 206GPa, respectively. The summary of all material properties are shown in **Table 2**.

The strengthening area of the CFRP laminates and the SRP laminates were 200mm² and 220mm², respectively. In all cases the width of laminates was 1200mm. Since the experimental mine at UMR is limited to charge weights not to exceed 2-3 kg, the reinforcement ratio was limited to levels that would permit testing under these charge limitations. As such, the reinforcement ratio provided was limited to 0.18%, which corresponds to the secondary reinforcement considerations.

Under the action of blast loads the effect of high strain rates was considered by applying a dynamic increase factor of 1.20 for the reinforcement bars and 1.25 for the concrete material properties (Mays and Smith, 1995). Based on the material properties, the equivalent moment-curvature relationships for the five slabs were calculated and are presented in Figure 3. Under the given reinforcement ratio, the yielding moment of the control slab was computed at 7.2kN-m and the cracking moment was 6.5kN-m. The moment-curvature relationships of slabs 2A and 2B are identical to each other because the CFRP laminates placed on the compressive face were ignored in the analysis. For the

same reason, the moment-curvature relationships for slabs 3A and 3B are also identical to each other.

PREDICTION OF BLAST LOADING

In this work, the shape of the blast pressure wave was schematically simplified as a triangular impulsive load, as shown in Figure 4 (FEMA, 2003). In this figure, the negative pressure was not considered in the analysis, but future work should include this effect. The principal parameters required to define the blast loading are the peak overpressure, P_s , and the duration of the blast impulse, t_d . Simple expressions can be used to relate these parameters to the charge weight and the standoff distance, expressed as W and R , respectively.

Blast Load Relations

The peak overpressure can be expressed as a function of Z , which is designated as the blast load scaled distance (Mays and Smith, 1995):

$$P_s = \frac{6.7}{Z^3} + 1 \text{ bar} \quad (P_s \geq 10 \text{ bar}) \quad (1)$$

$$P_s = \frac{0.975}{Z} + \frac{1.455}{Z^2} + \frac{5.85}{Z^3} - 0.019 \text{ bar} \quad (0.1 \leq P_s \leq 10 \text{ bar})$$

In this equation, the scaled distance, Z , is correlated to W and R by:

$$Z = \frac{R}{W^{1/3}} \quad (2)$$

wherein the standoff distance is measured in meters, and the charge weight is based on a TNT-mass equivalence measured in kilograms. The duration of the blast impulse, t_d , can be determined as a function of W and R , given by (Lam et al, 2004; Mays and Smith, 1995):

$$\log_{10} \left(\frac{t_d}{W^{1/3}} \right) \approx -2.75 + 0.27 \log_{10} \left(\frac{R}{W^{1/3}} \right) \quad (Z \geq 1.0) \quad (3)$$

$$\log_{10} \left(\frac{t_d}{W^{1/3}} \right) \approx -2.75 + 1.95 \log_{10} \left(\frac{R}{W^{1/3}} \right) \quad Z \leq 1.0$$

These equations were then used to correlate the charge weight and the stand-off distance to the load duration. In the next section, prediction of the charge weight and standoff distance necessary to impose a given damage level on the tested slabs was based on the principles of the DBD method to be discussed next.

Displacement Based Method Applied for Prediction of Blast Loads

An attractive feature of the DBD method is that the structural performance criteria selected for design or assessment can be correlated to a measurable quantity such as the displacement ductility. For RC members, displacement ductility levels in the range of 1 to 6 can be correlated to performance damage levels that either lead to “small cracks only” or to “major damage requiring repair”, respectively. These performance goals have been obtained based on test results, which confirm that these performance levels can be directly related to specific displacement ductility levels (Hose et al., 2000).

In applying the DBD method it is practical to convert the bilinear inelastic response of a given member to an idealized linear elastic response, as shown in Figure 5 (Priestley et al., 1995). According to this procedure the entire inelastic force-displacement response is described by an idealized linear elastic system with an equivalent stiffness, K_{eff} , such that the following holds true:

$$K_{eff} = \frac{F_a}{\Delta_a} \quad (4)$$

In assessment conditions the yield deflection, D_y , is easily computed and the selected displacement, Δ_a , can be obtained based on the selected performance level or ductility, μ , with:

$$\Delta_a = \mu \Delta_y \quad (5)$$

Based on the substitute structure shown in Figure 5, the capacity, F_a , at a given μ and for a given post-yield stiffness, r , can be derived based on the relation:

$$F_a = [r(\mu - 1) + 1]F_y \quad (6)$$

These three equations were used to completely describe the load-deformation response for the substitute structure. This method of converting the structural performance into a simplified response is often designated as the substitute structure approach (Priestley et al., 2000). Meanwhile, the corresponding equivalent elastic period, T_{eff} , is given by:

$$T_{eff} = 2\pi \sqrt{\frac{M}{K_{eff}}} \quad (7)$$

where M is the effective mass of the system.

Another parameter that must be used in dynamic analysis using the substitute structure approach is the equivalent viscous damping (EVD) ratio. Previous work (Lu and Silva, 2004) have correlated the EVD ratio, ξ_{eff} , as a function of the displacement ductility level for members under blast loads by the relation:

$$\xi_{eq} = 0.05 + \frac{1}{\pi} \frac{(1-r)(\mu-1)}{\mu[1+r(\mu-1)]} \quad (8)$$

Dynamic load effects can be correlated to an equivalent static load by a relation designated as the dynamic response factor (DRF) (Clough and Penzien, 1993):

$$DRF = \frac{\Delta_a}{\Delta_{st}} \quad (9)$$

where Δ_a is the same as the displacement selected for assessment under the imposed dynamic loads, and Δ_{st} is the static displacement, which is given by:

$$\Delta_{st} = \frac{P_s}{K_{eff}} \quad (10)$$

The expression to compute DRF developed for blast loads was given by (Lu and Silva, 2005):

$$DRF = e^{-\frac{\xi_{eff}}{\sqrt{1-\xi_{eff}^2}}\theta^*} \left(f_1 \cos \theta^* + \frac{\xi_{eff} f_1 + f_2}{\sqrt{1-\xi_{eff}^2}} \sin \theta^* \right) \quad (11)$$

where θ^* is the phase angle for the maximum displacement given by:

$$\theta^* = \tan^{-1} \left(\frac{f_2 \sqrt{1-\xi_{eff}^2}}{f_1 + \xi_{eff} f_2} \right) \quad (12)$$

In the expressions above, f_1 and f_2 are functions of the EVD, ξ_{eff} , and the non-dimensional time duration, t_d / T_{eff} , ratios given by:

$$f_1 \left(\xi_{eff}, \frac{t_d}{T_{eff}} \right) = -e^{-2\pi\xi_{eff}\frac{t_d}{T_{eff}}} \left[\left(1 + \frac{\xi_{eff}}{\pi \frac{t_d}{T_{eff}}} \right) \cos \left(2\pi \frac{t_d}{T_{eff}} \sqrt{1-\xi_{eff}^2} \right) + \frac{\xi_{eff}}{\pi \frac{t_d}{T_{eff}}} \right. \\ \left. + \frac{1}{\sqrt{1-\xi_{eff}^2}} \left(\xi_{eff} + \frac{2\xi_{eff}^2 - 1}{2\pi \frac{t_d}{T_{eff}}} \right) \sin \left(2\pi \frac{t_d}{T_{eff}} \sqrt{1-\xi_{eff}^2} \right) \right] \quad (13)$$

$$f_2 \left(\xi_{eff}, \frac{t_d}{T_{eff}} \right) = -e^{-2\pi\xi_{eff}\frac{t_d}{T_{eff}}} \left(\begin{array}{l} \left(2\xi_{eff} + \frac{4\xi_{eff}^2 - 1}{2\pi\frac{t_d}{T_{eff}}} \right) \cos \left(2\pi\frac{t_d}{T_{eff}}\sqrt{1-\xi_{eff}^2} \right) \\ - \frac{1}{\sqrt{1-\xi_{eff}^2}} \left(1 + \frac{\xi_{eff}}{2\pi\frac{t_d}{T_{eff}}} \right) \sin \left(2\pi\frac{t_d}{T_{eff}}\sqrt{1-\xi_{eff}^2} \right) \end{array} \right) + \frac{1}{2\pi\frac{t_d}{T_{eff}}} \quad (14)$$

Using the substitute structure approach for a single degree of freedom system with a given effective stiffness, K_{eff} , and an EVD ratio, ξ_{eff} , which can be correlated to a specified damage level, Figure 6 presents the numerical results for DRF as a function of the non-dimensional time ratio and under two different displacement ductility levels (1 and 4). The correlation between these displacement ductility levels and the EVD ratio were obtained in term of Eq. (8). Finally, using the blast load duration ratio, t_d/Te_{ff} , and the DRF obtained from Figure 6 the peak overpressure, P_s , can be determined as:

$$P_s = \frac{\Delta_a K_{eff}}{DRF} \quad (15)$$

Steps Used to Predict the Blast Charge and Standoff Distance

A general flow-chart for predicting the charge weight and the standoff distance is given in Figure 7.

The first step in this procedure consists of selecting the displacement ductility level that will be used for the assessment of the slabs. In this work, the two displacement ductility levels selected for predicting the blast loads were 1 and 4, corresponding to damage levels that can be identified by "minor cracks or no damage" to "visible cracks and crushing of the cover concrete". The ductility level selected for assessment of all the corresponding slabs are shown in Table 3. Since the strengthened slabs (2A-3B) respond within the elastic range up to failure, the ductility level for these slabs must be 1.

Steps 2 through 4 are self explanatory and can be related to the expressions previously described, as shown in Figure 7.

A primary strategy for protecting buildings is to ensure that a certain standoff distance is met such that the shock front generated by explosions decreases significantly with distance. In step 5 the standoff distance, R , is selected as shown in the flow-chart, and steps 6 through 9 are once again self explanatory and can be related to the expressions shown in Figure 7.

1352 Lu et al.

In step 10, when the difference between the value of t_d from step 6 and the value of t_{d1} computed in step 10 is within an acceptable degree of accuracy, the procedure is terminated. Otherwise, a new iteration cycle is performed by setting the value of t_d for step 6 as the value of t_{d1} obtained from step 10. Table 3 presents the final iteration and the corresponding steps. The test charge weights and the corresponding standoff distances used during blast testing of the five slabs are summarized in Table 4. Detailed research results are presented and discussed next.

RESULTS AND DISCUSSION

Slab 1 under First Event

The first event was generated by a charge weight of 0.45kg that was suspended above the center of the slab and placed at a standoff distance of 910mm, which corresponds to the $m=1$ damage level. From Figure 8a, as expected after this event no damage was observed on the control slab.

Slab 1 under Second Event

The second event was generated by a charge weight of 0.90kg, which was also suspended above the center of the slab and placed at a standoff distance of 300mm, which corresponds to the $m=4$ damage level. From Figure 8b, a major flexural crack was observed at the mid-span. The maximum crack width was 3mm. The residual displacement at the center of the slab was measured at 21mm, and the residual displacement at the mid-point along the edge was measured at 11mm. By assuming the residual displacement varies linearly from the center to the edges of the slab, the average residual displacement was calculated at nearly 14mm. Recognizing the yield displacement equals 4.1mm, the achieved displacement ductility level during test was 4.4 which is close to the predicted displacement ductility level. These results indicate that the charge weight and standoff distance were effectively estimated by using the DBD method.

Slab 2A

An explosive charge weight of 1.35kg was applied on this slab at a standoff distance of 300mm. As shown in Figure 9a, this slab was severely damaged under this explosive charge, and no residual deformation could be realistically measured. This result indicates that slabs retrofitted by CFRP laminates on the bottom side only are not adequate in increasing the blast-resistant capacity of slabs for the given threat level as a results of the dynamic response or negative overpressure.

Slab 2B

Slab 2B, was subjected to the same charge weight and standoff distance as slab 2A. Two major shear cracks were observed near the supports and no significant flexural cracks were observed, as shown in Figure 9b. The measured residual displacement was 44mm and 28mm at the center and at the mid span along the edges, respectively. By comparing the experimental results of slab 2B with 2A, it can be concluded that the flexural capacity under blast loads was increased by strengthening both sides. Future

testing should also consider the shear failure of the retrofitted slabs. This can be easily achieved by expanding the retrofit laminates to the edge of the slabs.

Slab 3A

Slab 3A, was also subjected to a blast load generated by a charge weight of 1.35kg and a standoff distance of 300mm. Figure 10a shows that this slab suffered significant damage under an explosive charge identical to slab 2A. This result indicates that slabs retrofitted by SRP laminates on the bottom side only are also not adequate in increasing the blast-resistant capacity of slabs.

Slab 3B

Slab 3B was also subjected to a blast load generated by a charge weight of 1.35kg and a standoff distance of 300mm. Two major shear cracks were observed near the supports and no significant flexural cracks were observed. As in slab 2B, future research should address this issue by extending the sheets to the edges of the slab. The measured residual displacement was 44mm and 28mm at the center and the mid span along the edges, respectively.

CONCLUSIONS

In this work, the blast charge weights and the standoff distances to impose a desired displacement ductility level were estimated based on the modified DBD method to account for blast effects. The results of field test for the control slab showed that the achieved displacement ductility levels matched closely with the predicted values. Therefore, a primary conclusion drawn from the experimental results is that the charge weight and standoff distance to generate blast loads can be effectively estimated by the DBD method according to the procedure presented in this paper.

Furthermore, slabs retrofitted on the bottom side only were severely damaged irrespective of the strengthening material. However, slabs retrofitted on both sides were adequate in resisting the given threat level; but, failure due to the insufficient shear capacity was observed. By comparing the test results of slabs strengthened on the bottom side and on both sides, the main conclusion was that slabs may require retrofitting on both sides in order to make these slabs resistant to blast loads.

ACKNOWLEDGMENTS

The analytical development of the DBD method presented in this paper was funded by the National Science Foundation under a small Grant for Exploratory Research Grant No. CMS-0335393. On the other hand, the field tests were funded by Structural Preservation Systems, through the NSF Industry/University Cooperative Research Center at the University of Missouri - Rolla. In addition the authors would also like to thank Hardwire, LLC for their donation of the steel tapes.

REFERENCES

- Clough, R.W., and Penzien. J. (1993), *Dynamics of Structures*, 2nd Edition, McGraw Hill Inc., New York, NY, 1993, 635 pp.
- Federal Emergency Management Agency, (FEMA) (2003) "FEMA 426- Reference Manual to Mitigate Potential Terrorist Attacks Against Buildings" FEMA-426, December 2003.
- Hose, Y. D., Silva, P. F., Seible, F. (2000), "Performance Evaluation of Concrete Bridge Components and Systems under Simulated Seismic Loads," *EERI Earthquake Spectra*, Vol. 16, No. 2, May 2000, pp. 413-442.
- Lam, N.; Mendis, P., Ngo, T. (2004) "Response Spectrum Solution for Blast Loading." *Electronic Journal of Structural Engineering*, 4(2004) pp.28-44
- Lu, B.; and Silva, P. (2004) "Estimating Equivalent Viscous Damping Ratio For RC Members under different loading Types", *Mechanics Research Communications*; Submitted.
- Lu, B.; and Silva, P. (2005) "Inelastic Shock Spectra for Blast Loads", *Mechanics Research Communications*; Submitted.
- Mays, G. C. and Smith, P. D. (1995) *Blast Effects on Buildings*, Thomas Telford Service Ltd, London, E14 4JD. 121pp.
- Priestley, M.J.N. (2000), .Performance Based Seismic Design,. *Proceedings of the 12th World Conference on Earthquake Engineering*, Auckland, New Zealand, 2000, State of the Art Paper No. 2831, pp. 325-346.
- Priestley, M. J. N., Seible, F., and Calvi, M.,(1995) *Seismic Design and Retrofit of Bridges*, John Wiley & Sons, Inc., New York, NY, Sep 1995, 672 pp.
- Wobbe, E., Silva, P, and Barton, B. et al (2004), "Flexural Capacity of RC Beams Externally Bonded with SRP and SRG" ACI Conference, San Francisco, CA, November, 2004

Table 1 Experimental Test Matrix

Slab No.	Strengthening scheme
1	Control (None)
2A	CFRP (1 side, bottom)
2B	CFRP (2 sides)
3A	SRP(1 side, bottom)
3B	SRP(2 sides)

Table 2 Material Properties of CFRP and SRP

	Tensile strength (MPa)	Elastic modulus (GPa)	Ultimate strain (%)	Strengthening Area (mm ²)
CFRP	3794	228	1.7	200
SRP	3199	206	1.6	220

Table 3 Standoff Distance and Estimated Charge Weight of Blast Loads

Step No.	1	2	3			4	5	6	7	8	9	10
Damage level	m	ξ_{eff} (%)	D_a (mm)	F_a (kN)	K_{eff} (kN/m)	T_{eff} (sec)	R (mm)	t_d (sec)	DRF	P_s (bar)	W (kg)	t_d (sec)
No damage	1	5	4.1	20.5	5040	0.04	910	0.0014	0.110	5.0	0.44	0.0014
Major crack	4	30	16.4	20.5	1260	0.07	300	0.00018	0.005	215	0.91	0.00018
Ultimate (CFRP)	1	5	16.5	133.5	8155	0.03	300	0.00016	0.021	322	1.33	0.00016
Ultimate (SRP)	1	5	16.4	125.5	7718	0.03	300	0.00016	0.020	322	1.30	0.00016

Table 4 Applied Charges and Standoff Distances

Shot No.	Slab No.	Charge Weights (kg)	Standoff Distances (mm)
1	1	0.45	910
2	1	0.90	300
3	2A	1.35	300
4	2B	1.35	300
5	3A	1.35	300
6	3B	1.35	300

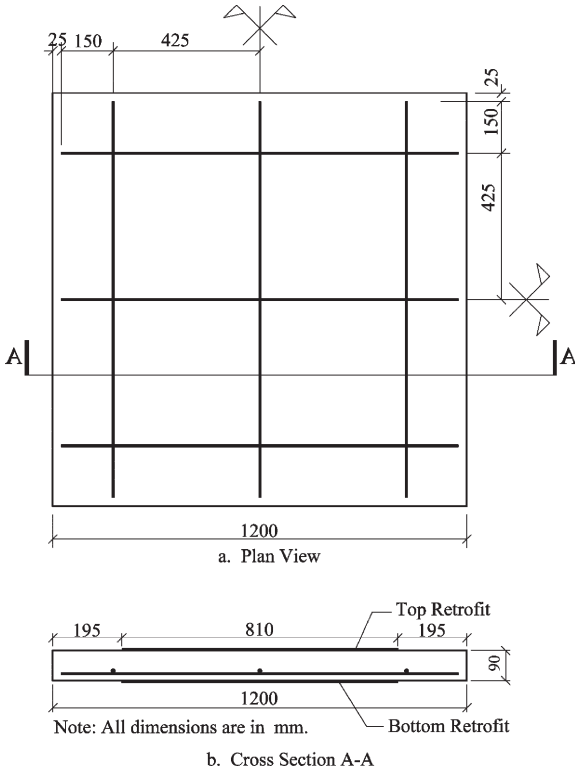


Figure 1 RC Slab and Reinforcement Detail

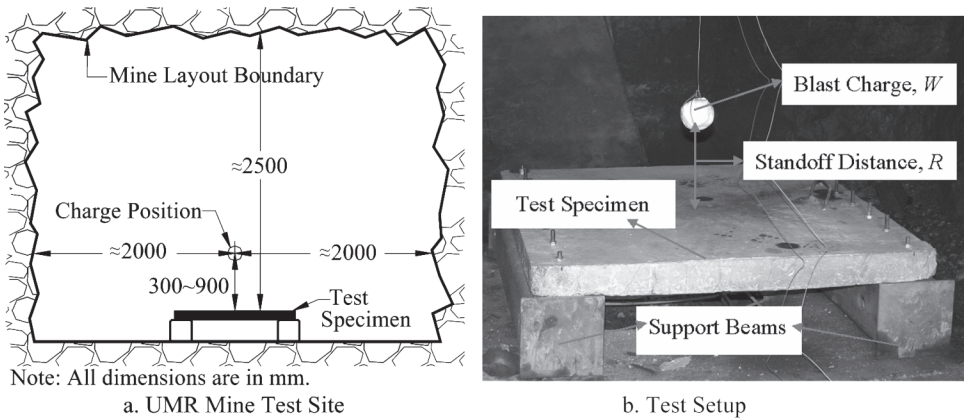


Figure 2 Test Site and Test Setup

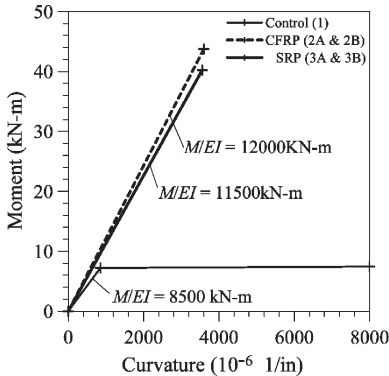


Figure 3 Moment- Curvature Relationship

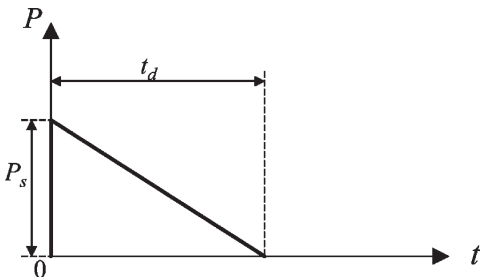


Figure 4 Simplified Pressure-Time Profile for Blast

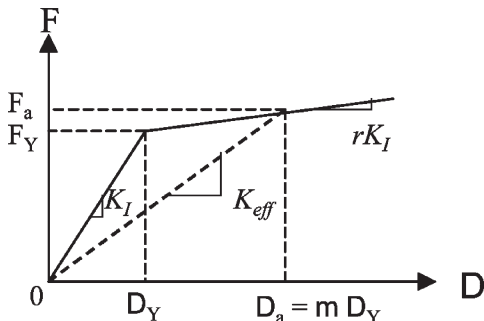


Figure 5 Substitute Structure Model

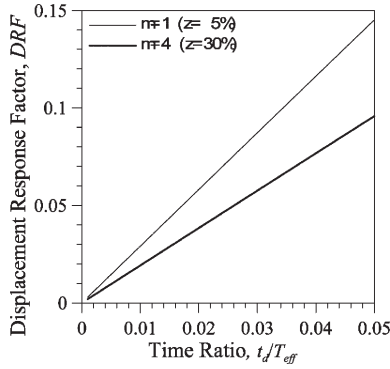


Figure 6 Displacement Response Factor for Simplified Blast Load

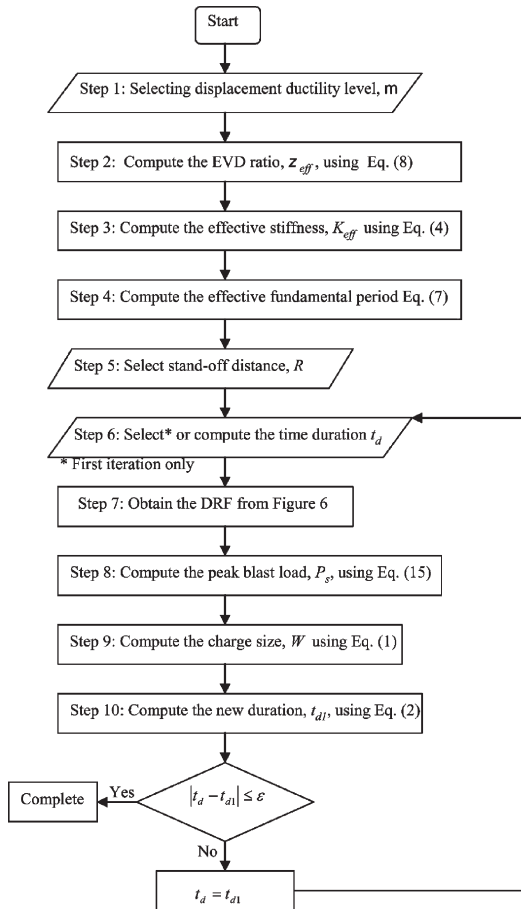
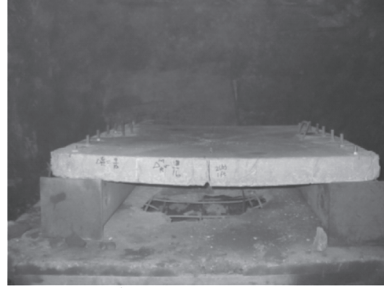


Figure 7 Flow Chart for Predicting Blast Loads



a. 1st Event (0.45kg, 910mm)

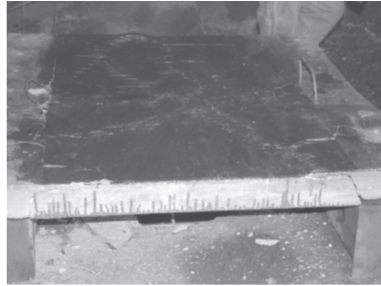


b. 2nd Event (0.9kg, 300mm)

Figure 8 Experimental Results for Control Slab



a. 2A (1.35kg, 300mm)



b. 2B (1.35kg, 300mm)

Figure 9 Experimental Results for CFRP Retrofitted Slabs



a. 3A (1.35kg, 300mm)



b. 3B (1.35kg, 300mm)

Figure 10 Experimental Results for SRP Retrofitted Slabs

